Japanese Journal of Applied Physics

The Japan Society of Applied Physics

REGULAR PAPERS

Fabrication and leakage current and ferroelectric characteristics of multiferroic Fe_3O_4/($Bi_{3.25}Nd_{0.65}Eu_{0.10}$)$Ti_3O_{12}$ composite thin films with Fe_3O_4 magnetic electrodes micropatterned by reactive ion etching

To cite this article: Masafumi Kobune *et al* 2017 *Jpn. J. Appl. Phys.* **56** 10PF02

Japanese Journal of Applied Physics 56, 10PF02 (2017)
https://doi.org/10.7567/JJAP.56.10PF02

REGULAR PAPER

Fabrication and leakage current and ferroelectric characteristics of multiferroic $Fe_3O_4/(Bi_{3.25}Nd_{0.65}Eu_{0.10})Ti_3O_{12}$ composite thin films with Fe_3O_4 magnetic electrodes micropatterned by reactive ion etching

Masafumi Kobune[1]*, Takuya Nishimine[1], Takuya Matsunaga[1], Satoshi Fujita[1], Takeyuki Kikuchi[1], Hironori Fujisawa[2], Masaru Shimizu[2], Kensuke Kanda[2], and Kazusuke Maenaka[2]

[1]Department of Chemical Engineering and Materials Science, Graduate School of Engineering, University of Hyogo, Himeji, Hyogo 671-2201, Japan
[2]Department of Electrical Engineering and Computer Sciences, Graduate School of Engineering, University of Hyogo, Himeji, Hyogo 671-2201, Japan

*E-mail: kobune@eng.u-hyogo.ac.jp

Received May 26, 2017; accepted July 11, 2017; published online September 7, 2017

Regardless of the deposition time (30–90 min), almost single-phase magnetite (Fe_3O_4) films with a cubic inverse-spinel structure were produced at a substrate temperature of 500 °C by metalorganic chemical vapor deposition (MOCVD). The $Fe_3O_4/(Bi_{3.25}Nd_{0.65}Eu_{0.10})Ti_3O_{12}$ (BNEuT) composite film deposited at 500 °C for 90 min by MOCVD exhibited excellent room-temperature magnetic properties, such as a saturation magnetization of 480 emu/cm^3, a residual magnetization of 160 emu/cm^3, and a coercivity of 297 Oe. Ferromagnetic Fe_3O_4 electrodes micropatterned using a combination of photolithography and reactive ion etching were fabricated after MOCVD, and their structural, leakage current, and ferroelectric characteristics were investigated. The room-temperature leakage current density–applied electric field and polarization–electric field (*P*–*E*) characteristics of the composite films were successfully measured using Fe_3O_4 electrodes. The room-temperature *P*–*E* hysteresis loop for a sample with the structure Fe_3O_4/BNEuT/Nb:TiO_2/Ti had a relatively good shape, with a remanent polarization of 8 μC/cm^2 and a coercive field of 193 kV/cm.

1. Introduction

To minimize clamping effects[1–3] due to the presence of a substrate, and achieve enhanced multiferroic (MF) properties (ferroelectricity and ferromagnetism) and a large magneto-electric (ME) effect,[4–8] we fabricated nanopillar-type MF composite devices by depositing the ferromagnetic material magnetite (Fe_3O_4)[9–14] on (200) $(Bi_{3.25}Nd_{0.65}Eu_{0.10})Ti_3O_{12}$ (BNEuT)/(101) Nb:TiO_2 substrates[15–17] by metalorganic chemical vapor deposition (MOCVD)[18,19] in our previous study.[20] We succeeded in achieving a high magnetite particle filling rate of approximately 90% in narrow spaces between BNEuT nanoplates. The substrate temperature during MOCVD was found to be the dominant factor influencing both the filling rate and the crystallinity of the magnetite particles. It is known that Fe_3O_4 has a cubic inverse-spinel structure (space group: $Fd\bar{3}m$)[21] above the so-called Verwey transition temperature of 120 K.[22,23] A film with a thickness of 100 nm was found to exhibit a room-temperature electrical conductivity of 2.38×10^2 S/cm, which is as high as that of metals.[24] It also displayed excellent room-temperature ferromagnetism with a large saturation magnetization (M_s) of 479 emu/cm^3[3,9] and a comparatively small coercivity (H_c) of 200–400 Oe.[23] Although these properties make such films promising for use in magnetic electrodes at temperatures of 120–858 K,[23] it is necessary to develop an effective electrode micropatterning process in order to investigate the electrical properties of the composite devices. In the present study, we examine the feasibility of high-speed, accurate micropatterning of Fe_3O_4 films on BNEuT/Nb:TiO_2 substrates by reactive ion etching (RIE).[25–28] Kanda and coworkers reported the use of RIE to fabricate multimorph cantilevers with a stacked structure comprising alternate piezoelectric Pb(Zr,Ti)O_3 and internal Pt/Ti/Pt electrode layers.[29–32] The devices generated a larger force than conventional unimorph and bimorph cantilevers. However, there have been no reports on the fabrication of ferromagnetic Fe_3O_4 film electrodes micropatterned by RIE thus far.

In the present study, multiferroic Fe_3O_4/BNEuT composite thin films were fabricated by depositing ferromagnetic Fe_3O_4 films with different thicknesses on (200) BNEuT/(101) Nb:TiO_2 substrates by MOCVD and varying the deposition time. The Fe_3O_4 films were then micropatterned to produce electrodes using a combination of photolithography and RIE. The structural, leakage current, and ferroelectric characteristics of the RIE-processed composite films were then investigated.

2. Experimental procedure

BNEuT ferroelectric template films were deposited on (101) Nb:TiO_2 substrates using an rf sputtering equipment.[15–17] Fe_3O_4 films were deposited by MOCVD using iron(III) tris(2,2,6,6-tetramethyl-3,5-heptanedionato) [Fe(thd)$_3$][33,34] as the metalorganic precursor. The MOCVD system had a single metalorganic precursor delivery system, and has been described in detail elsewhere.[20] Each film was deposited on a 1.9-μm-thick (200) BNEuT/(101) Nb:TiO_2 substrate at a substrate temperature of 500 °C under a carrier gas flow rate of 100 sccm and an oxidizing gas flow rate of 300 sccm. To investigate the effects of the Fe_3O_4 electrode thickness on the electrical properties of the composite films, deposition times of 30, 60, and 90 min were used. Figures 1(a) and 1(b) show the schematic illustrations of as-deposited and RIE-processed composite films, respectively. The thicknesses of the Fe_3O_4 layers deposited for 30, 60, and 90 min were approximately 70, 140, and 210 nm, respectively. A schematic illustration of the MOCVD and RIE processes for fabricating micro-patterned Fe_3O_4 film electrodes on BNEuT/Nb:TiO_2 substrates is shown in Fig. 2. After spin-coating the Fe_3O_4/BNEuT sample with a photoresist layer, it was patterned using a photomask containing circular holes with diameters of 30, 50, 100, and 200 μm in a Canon PLA-501 photolithography system. Following the development of the photoresist, the exposed Fe_3O_4 regions were processed using a commercial ICP-RIE system (SAMCO RIE-101HU) under the etching conditions listed in Table I.

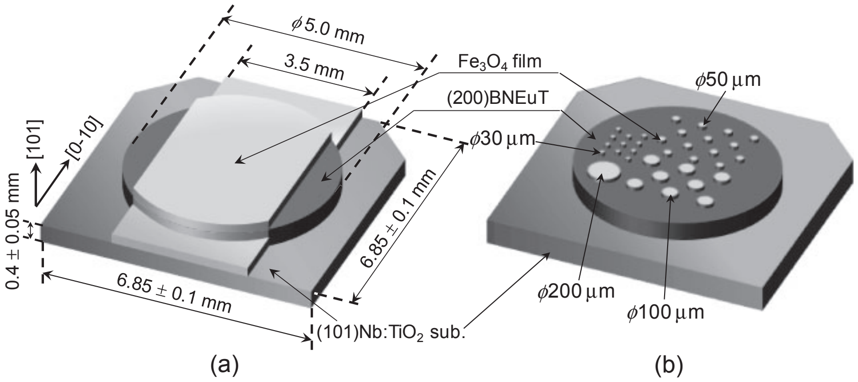

Fig. 1. Schematic illustrations of Fe_3O_4/BNEuT composite thin films deposited by MOCVD: (a) as-deposited and (b) RIE processed.

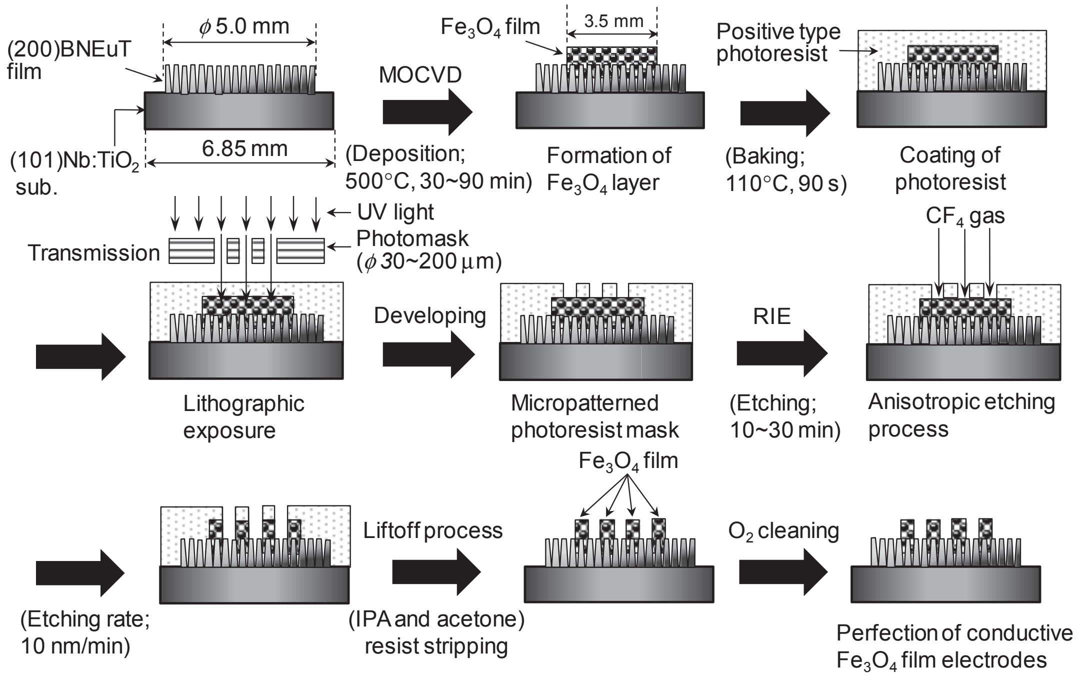

Fig. 2. Schematic illustration of MOCVD and RIE processes for fabricating micropatterned Fe_3O_4 film electrodes on (200) BNEuT/(101) Nb:TiO_2 substrates.

Table I. Etching conditions for micropatterning Fe_3O_4 electrodes by RIE.

Reactive gas	CF_4
Flow rate of reactive gas (sccm)	20
Rf power for plasma generation (W)	300
Rf bias power (W)	50
Process pressure (Pa)	2
Etching rate (nm/min)	10

Phase identification in the composite films was conducted by X-ray diffraction (XRD; Rigaku Ultima IV). The observations of the surface microstructure of the as-deposited films and the Fe-Kα and Bi-Mα elemental mapping of the films following RIE processing were performed by field-emission scanning electron microscopy (FE-SEM; JEOL JSM-7001FA) combined with energy-dispersive X-ray spectroscopy (EDS). Magnetic moment–magnetic field (m–H) curves for the samples were measured at room temperature using a vibrating sample magnetometer (Toei Industry VSM-5).[35–38] A magnetic field of 0 to ± 5 kOe was applied in the plane of the samples. The magnetization (M) was calculated as $m \cdot \rho / w$, where m is the magnetic moment, ρ is the density ($5.195 \times 10^3\,\mathrm{kg/m^3}$) estimated from the theoretical volume and molecular weight of polycrystalline Fe_3O_4,[39] and w is the Fe_3O_4 mass determined from measurements using an ultra-microbalance (Mettler Toledo XP2U) before and after Fe_3O_4 deposition. To form ohmic contacts for electrical measurements, rf sputtering without substrate heating was carried out to deposit a 30-nm-thick Ti film[40] on the back side of the substrate. The samples used to measure the leakage current density–applied electric field (J–E) and ferroelectric characteristics thus had the structure Fe_3O_4/BNEuT/Nb:TiO_2/Ti. The J–E characteristics were measured at room temperature under an applied field that was swept from 0 to 250 kV/cm in 10 kV/cm steps, at 10 s intervals using a programmable electrometer (Keithley 617). Polarization–electric field (P–E) hysteresis loops were measured at room temperature using a ferroelectric test system (Toyo FCE3-EMS).

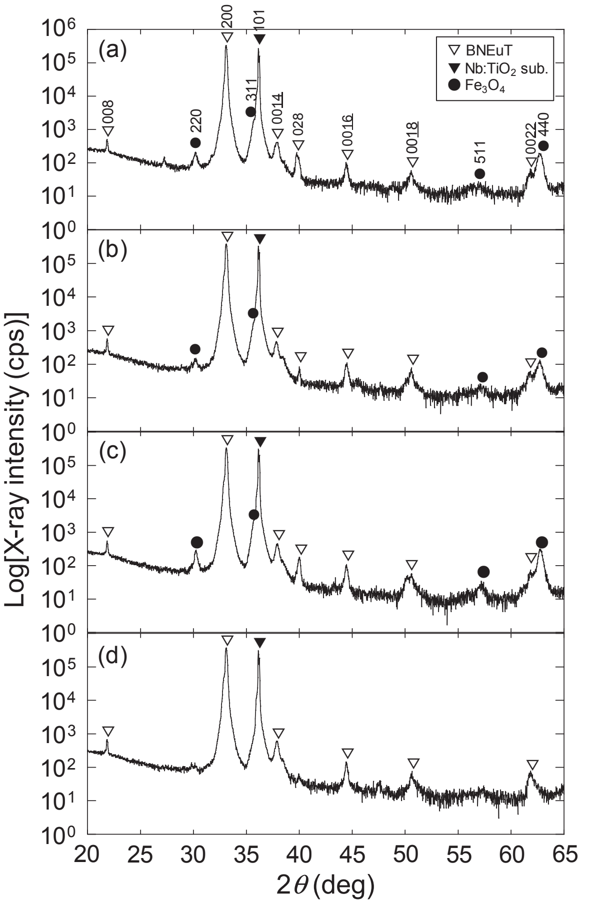

Fig. 3. XRD profiles for iron oxide films deposited at 500 °C for (a) 30, (b) 60, and (c) 90 min by MOCVD, and (d) typical (200) BNEuT/(101) Nb:TiO_2 substrate before MOCVD deposition.

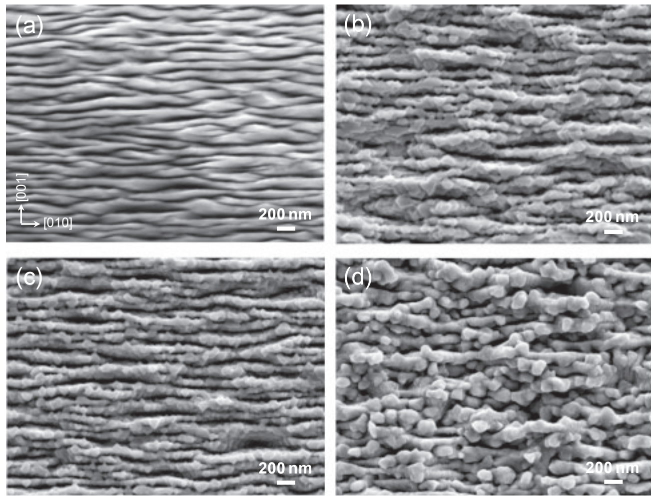

Fig. 4. Surface FE-SEM images of (a) sputtered BNEuT thin film used as ferroelectric template and Fe_3O_4/BNEuT composite thin films deposited at 500 °C for (b) 30, (c) 60, and (d) 90 min by MOCVD.

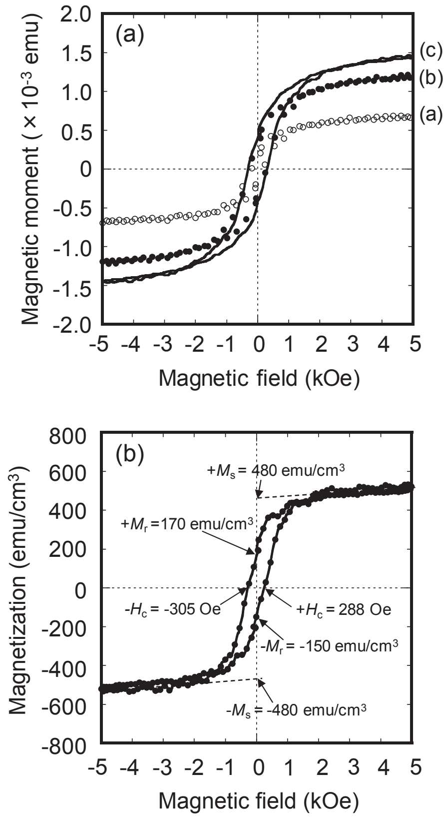

Fig. 5. (a) Room-temperature in-plane *m–H* curves for Fe_3O_4/BNEuT composite films deposited at 500 °C for (a) 30, (b) 60, and (c) 90 min, and (b) room-temperature in-plane *M–H* curve for a Fe_3O_4/BNEuT composite film deposited at 500 °C for 90 min by MOCVD.

3. Results and discussion

Figure 3 shows XRD profiles for composite films following iron oxide deposition for (a) 30, (b) 60, and (c) 90 min by MOCVD, and (d) a typical BNEuT/Nb:TiO_2 substrate before MOCVD deposition. As can be seen, the BNEuT films used as ferroelectric templates exhibit a strong 200 diffraction peak and relatively weak 00*l* peaks; the degree of *a*-axis orientation was calculated to be approximately 98.5%. In Figs. 3(a)–3(c), the deposited iron oxide is observed to consist of mainly single-phase Fe_3O_4 with a cubic inverse-spinel structure,[21] regardless of the deposition time. The existence of 220, 311, 511, and 440 diffraction peaks suggests that the Fe_3O_4 is polycrystalline, which is consistent with the ring-like selected area electron diffraction patterns observed in our previous study.[20]

Figure 4 shows the surface FE-SEM images of (a) a BNEuT ferroelectric template film and Fe_3O_4/BNEuT composite films deposited for (b) 30, (c) 60, and (d) 90 min by MOCVD. Figure 4(a) shows characteristic BNEuT nanoplates with a height of 1.9 μm and a width of 50–100 nm stacked along the [001] direction. As seen in Figs. 4(b) and 4(c), for Fe_3O_4 deposition times of 30 and 60 min, the surface morphologies are similar, consisting of ferromagnetic grains with diameters of 110–150 nm thinly coating both surfaces of the nanoplates while maintaining the underlying nanoplate shape. On the other hand, at 90 min, agglomerated particles comprising grains with an average diameter of approximately 190 nm are observed in Fig. 4(d). The latter result is seen to be produced according to MOCVD growth that is a diffusion-limited process determined by the rate of arrival of raw material gases and the rate of desorption of unnecessary produced gases, as described in detail elsewhere.[20]

Figure 5(a) shows room-temperature in-plane *m–H* curves for composite films produced by Fe_3O_4 deposition for (a) 30, (b) 60, and (c) 90 min, and Fig. 5(b) shows a room-temperature in-plane *M–H* curve for the composite film produced

Table II. Relationship between hole diameter in photomask and RIE accuracy.

MOCVD time (min)	30	60	90
Fe_3O_4 film thickness (nm)	70	140	210
Hole diameters in photomask (μm) (Theoretical values)	Average diameters for RIE-processed electrodes (μm) [comparison with theoretical values (%)][a]		
30	30.2 [100.6]	30.1 [100.4]	31.3 [104.3]
50	49.9 [99.8]	49.4 [98.7]	50.0 [100.0]
100	98.4 [98.4]	97.6 [97.6]	98.0 [98.0]
200	196.2 [98.1]	195.2 [97.6]	195.2 [97.6]

a) {[measured average values]/[theoretical values]} × 100.

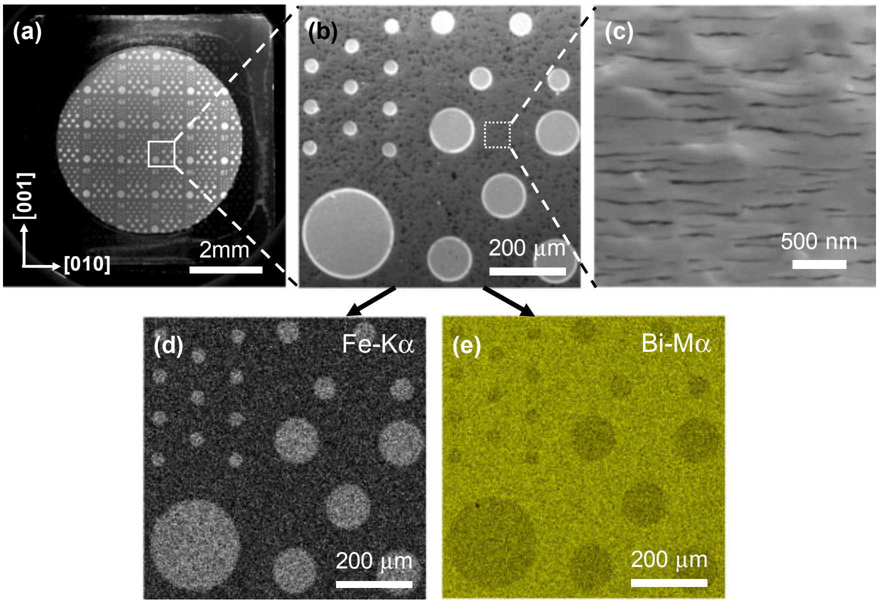

Fig. 6. (Color online) (a) Surface FE-SEM image of composite thin film, following Fe_3O_4 deposition at 500 °C for 90 min by MOCVD and RIE for 30 min, (b) enlarged image showing circular electrodes, (c) high-magnification image of RIE-processed region, and EDS elemental maps using (d) Fe-Kα peak at 6.398 keV (white color) and (e) Bi-Mα peak at 2.419 keV (yellow color) for the region shown in (b).

by Fe_3O_4 deposition for 90 min. As seen in Fig. 5(a), all of the samples exhibit narrow rectangular hysteresis loops, indicating that these materials are ferromagnetic, and the room-temperature saturation magnetic moments are 0.56×10^{-3}, 1.00×10^{-3}, and 1.21×10^{-3} emu for deposition times of 30, 60, and 90 min, respectively. Furthermore, the residual magnetic moment (m_r) increases with the deposition time. This can be attributed to the increase in the amount of Fe_3O_4 with increasing deposition time. As shown in Fig. 5(b), the composite film produced by Fe_3O_4 deposition for 90 min exhibited excellent magnetic properties, such as an M_s of 480 emu/cm^3, a residual magnetization (M_r) of 160 emu/cm^3, and a H_c of 297 Oe. The M_s value is in good agreement with the value of 479 emu/cm^3 for (100)-oriented Fe_3O_4 films produced by reactive sputtering on (100) MgO substrates.[9] In addition, the H_c value is consistent with the values of 200–400 Oe previously reported for epitaxial Fe_3O_4 films deposited on (100) MgO and (110) MgO substrates by pulsed laser deposition.[23] Therefore, it is expected that the composite film can be used as a soft magnetic material for ferromagnetic applications.

To fabricate micropatterned Fe_3O_4 film electrodes on the BNEuT/Nb:TiO_2 substrates, RIE was carried out. RIE is thought to involve a two-step reaction: 1) $2CF_4 \rightarrow 4F^- + 2CF_2^{2+}$ and 2) $Fe_3O_4 + 4F^- + 2CF_2^{2+} \rightarrow FeF_2 + 2FeF_3 + 2CO_2$. The reaction products (FeF_2 and FeF_3) and CO_2 gas are removed from the chamber via an exhaust system. Figure 6(a) shows a surface FE-SEM image of a composite film produced by Fe_3O_4 deposition for 90 min, following RIE patterning for 30 min. Figure 6(b) shows an enlarged image, where the circular Fe_3O_4 electrode regions can clearly be seen. Figure 6(c) shows a high-magnification image of a region processed by RIE to remove the Fe_3O_4 film. The EDS elemental maps of the region in Fig. 6(b) obtained using the Fe-Kα and Bi-Mα peaks are shown in Figs. 6(d) and 6(e), respectively. The RIE accuracy is given in Table II. The highest RIE accuracy was achieved for holes with a diameter of 50 μm, and the accuracy decreased with increasing hole diameter, regardless of the Fe_3O_4 deposition time. In Fig. 6(c), it is clear that the etched surface between the electrodes consists of the underlying BNEuT nanoplates. Also, the elemental maps in Figs. 6(d) and 6(e) show that the electrode regions contain a high level of Fe, whereas the region between them contains a high level of Bi; these results are consistent with the presence of Fe_3O_4 and BNEuT, respectively, and indicate that the Fe_3O_4/BNEuT composite films could be successfully micropatterned by RIE.

Using the micropatterned Fe_3O_4 electrodes with a diameter of 200 μm, the measurements of room-temperature J–E characteristics were carried out. Figure 7(a) shows the results

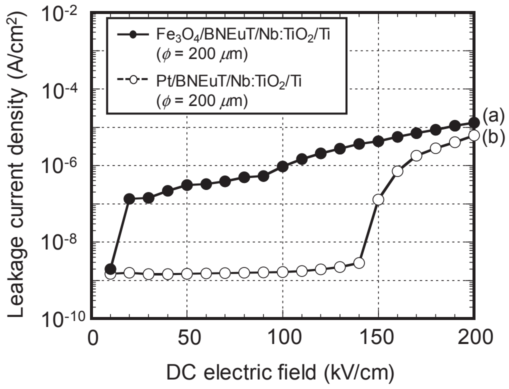

Fig. 7. Room-temperature *J–E* characteristics measured using 200-μm-diameter electrodes for samples with the structures (a) Fe_3O_4/BNEuT/Nb:TiO_2/Ti and (b) Pt/BNEuT/Nb:TiO_2/Ti for comparison.

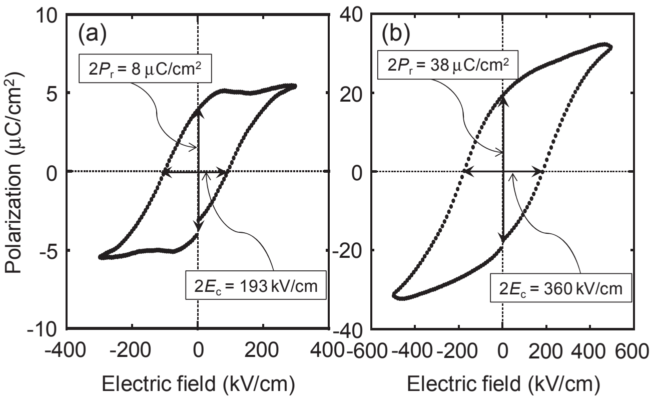

Fig. 8. Room-temperature *P–E* hysteresis loops for samples with the structures (a) Fe_3O_4/BNEuT/Nb:TiO_2/Ti and (b) Pt/BNEuT/Nb:TiO_2/Ti for comparison.

for a sample with the structure Fe_3O_4/BNEuT/Nb:TiO_2/Ti, and for comparison, Fig. 7(b) shows those for a sample with the structure Pt/BNEuT/Nb:TiO_2/Ti, which had a Pt electrode with a diameter of 200 μm. A positive bias was applied to the top electrode, thus producing an electric field that was parallel to the major polarization direction of the BNEuT films, as demonstrated using piezoresponse scanning force microscopy in our previous study.[20] The leakage current density for both samples was relatively low, at less than approximately 1×10^{-5} A/cm^2 under an applied field of up to 200 kV/cm. The electrical insulating properties of both samples were thus judged to be sufficiently high to evaluate their ferroelectric properties.

Figures 8(a) and 8(b) show room-temperature *P–E* hysteresis loops for the Fe_3O_4/BNEuT/Nb:TiO_2/Ti and Pt/BNEuT/Nb:TiO_2/Ti samples, respectively. The sample (a) was fabricated by RIE after MOCVD, while the sample (b) was fabricated without RIE by rf sputtering to form the Pt top electrodes on BNEuT/Nb:TiO_2 substrates. Both samples exhibited relatively good hysteresis loop shapes, with remanent polarization ($2P_r$) values of (a) 8 and (b) 38 μC/cm^2, and coercive field ($2E_c$) values of (a) 193 and (b) 360 kV/cm, respectively. The $2P_r$ value in Fig. 8(a) is approximately one-fifth that in Fig. 8(b), which is considered to be due to RIE that relaxes the thermal strain between the Fe_3O_4 layer and the BNEuT layer and/or in the BNEuT layer, resulting in the degradation of the polarization. Therefore, it can be expected that micropatterned Fe_3O_4/BNEuT composite thin films with excellent *M–H* and *P–E* characteristics can be realized by further optimizing the RIE conditions, such as the species and flow rate of reactive gas.

4. Conclusions

Ferromagnetic Fe_3O_4 thin films were deposited on (200) BNEuT/(101) Nb:TiO_2 substrates at 500 °C for 30–90 min by MOCVD, and their structural and magnetic characteristics were investigated. Subsequently, Fe_3O_4 electrodes micropatterned using a combination of photolithography and RIE were fabricated on (200) BNEuT/(101) Nb:TiO_2 substrates, and their structural, leakage current and ferroelectric characteristics were investigated. The following results were obtained:

(1) Regardless of the Fe_3O_4 deposition time (30–90 min), almost single-phase Fe_3O_4 films with a cubic inverse-spinel structure were produced.

(2) The Fe_3O_4/BNEuT composite film deposited at 500 °C for 90 min by MOCVD exhibited excellent room-temperature magnetic properties, such as an M_s of 480 emu/cm^3, an M_r of 160 emu/cm^3, and a H_c of 297 Oe.

(3) The room-temperature *J–E* and *P–E* characteristics of the composite films were successfully measured using the Fe_3O_4 electrodes.

(4) The room-temperature *P–E* hysteresis loop for a sample with the structure Fe_3O_4/BNEuT/Nb:TiO_2/Ti had a relatively good shape, with a $2P_r$ of 8 μC/cm^2 and a $2E_c$ of 193 kV/cm.

Acknowledgements

This work was supported in part by a Grant-in-Aid for Scientific Research B (No. 26289275) from the Japan Society for the Promotion of Science (JSPS) and the Academic–Industry Partnership Research Grant 2016 from Himeji City, Japan.

1) B. Fu, R. Lu, K. Gao, Y. Yang, and Y. Wang, EPL **112**, 27002 (2015).
2) A. R. Damodaran, J. C. Agar, S. Pandya, Z. Chen, L. Dedon, R. Xu, B. Apgar, S. Saremi, and L. W. Martin, J. Phys.: Condens. Matter **28**, 263001 (2016).
3) R. N. Torah, S. P. Beeby, and N. M. White, J. Phys. D **37**, 1074 (2004).
4) G. Lawes and G. Srinivasan, J. Phys. D **44**, 243001 (2011).
5) M. Li, Z. Zhou, M. Liu, J. Lou, D. E. Oates, G. F. Dionne, M. L. Wang, and N. X. Sun, J. Phys. D **46**, 275001 (2013).
6) F. Fang, Y. Y. Zhou, Y. T. Xu, W. Q. Jing, and W. Yang, Smart Mater. Struct. **22**, 075009 (2013).
7) J. Chen, C. Lin, Y. Yang, L. Hu, and W. Cheng, Modelling Simulation Mater. Sci. Eng. **22**, 015008 (2014).
8) N. Ortega, A. Kumar, J. F. Scott, and R. S. Katiyar, J. Phys.: Condens. Matter **27**, 504002 (2015).
9) D. T. Margulies, F. T. Parker, and A. E. Berkowitz, J. Appl. Phys. **75**, 6097 (1994).
10) X. W. Li, A. Gupta, G. Xiao, and G. Q. Gong, J. Appl. Phys. **83**, 7049 (1998).
11) S. Mathur, V. Sivakov, H. Shen, S. Barth, C. Cavelius, A. Nilsson, and P. Kuhn, Thin Solid Films **502**, 88 (2006).
12) S. Tiwari, R. J. Choudhary, R. Prakash, and D. M. Phase, J. Phys.: Condens. Matter **19**, 176002 (2007).
13) H. Yanagihara, M. Myoka, D. Isaka, T. Niizeki, K. Mibu, and E. Kita, J. Phys. D **46**, 175004 (2013).
14) H. Yanagihara, K. Shimada, T. Niizeki, E. Kita, J. Inoue, A. Fukushima, and S. Yuasa, J. Appl. Phys. **113**, 17B104 (2013).
15) M. Kobune, Y. Kaneko, R. Kishimoto, T. Kugimiya, S. Ueshima, H.

Nishioka, T. Kikuchi, H. Fujisawa, S. Nakashima, M. Shimizu, N. Fukumuro, and H. Matsuda, Jpn. J. Appl. Phys. **52**, 09KA10 (2013).
16) M. Kobune, T. Kugimiya, Y. Kaneko, S. Ueshima, T. Kikuchi, N. Fukumuro, H. Matsuda, K. Fukushima, H. Fujisawa, S. Nakashima, and M. Shimizu, Jpn. J. Appl. Phys. **53**, 02BC07 (2014).
17) M. Kobune, T. Kuriyama, R. Furotani, T. Kugimiya, S. Ueshima, T. Kikuchi, H. Fujisawa, S. Nakashima, M. Shimizu, and N. Fukumuro, Jpn. J. Appl. Phys. **54**, 10NA01 (2015).
18) K. Shalini, G. N. Subbanna, S. Chandrasekaran, and S. A. Shivashankar, Thin Solid Films **424**, 56 (2003).
19) S. Huang, S. Gu, K. Tang, J. Ye, Z. Xu, S. Zhu, and Y. Zheng, J. Vac. Sci. Technol. B **32**, 052801 (2014).
20) M. Kobune, R. Furotani, S. Fujita, K. Kikuchi, T. Kikuchi, H. Fujisawa, M. Shimizu, and N. Fukumuro, Jpn. J. Appl. Phys. **55**, 10TA01 (2016).
21) M. Paul, D. Kufer, A. Müller, A. Ruff, M. Kamp, N. J. C. Ingle, M. Sing, and R. Claessen, J. Appl. Phys. **110**, 073519 (2011).
22) A. Kumar, D. K. Pandya, and S. Chaudhary, J. Appl. Phys. **111**, 073901 (2012).
23) O. Chichvarina, T. S. Herng, W. Xiao, X. Hong, and J. Ding, J. Appl. Phys. **117**, 17D722 (2015).
24) R. Mantovan, S. Vangelista, S. Cocco, A. Lamperti, and O. Salicio, J. Appl. Phys. **111**, 07B107 (2012).
25) V. Bliznetsov, B. H. B. Johari, M. T. Chentir, W. H. Li, L. Y. Wong, S. Merugu, X. L. Zhang, and N. Singh, J. Micromech. Microeng. **23**, 117001 (2013).
26) M. Gharooni, A. Mohajerzadeh, A. Sanoughsaz, S. Khanof, S. Mohajerzadeh, and E. A. Soleimani, J. Micromech. Microeng. **23**, 095014 (2013).
27) J. Jung, S. Kim, W. Lee, and H. Choi, J. Micromech. Microeng. **23**, 125037 (2013).
28) J. M. Yoo, J. I. Song, P. Tathireddy, F. Solzbacher, and L. W. Rieth, J. Micromech. Microeng. **22**, 105036 (2012).
29) K. Kanda, S. Kajimura, J. Inoue, T. Fujita, and K. Maenaka, IEEJ Trans. Sens. Micromach. **134**, 18 (2014).
30) J. Inoue, K. Kanda, T. Fujita, and K. Maenaka, J. Micromech. Microeng. **25**, 055001 (2015).
31) K. Kanda, S. Moriue, T. Fujita, and K. Maenaka, Smart Mater. Struct. **26**, 045019 (2017).
32) R. Sano, J. Inoue, K. Kanda, T. Fujita, and K. Maenaka, Jpn. J. Appl. Phys. **54**, 10ND03 (2015).
33) V. N. Naumov, A. V. Seryakov, G. I. Frolova, V. V. Nogteva, P. A. Stabnikov, I. K. Igumenov, and M. A. Bespyatov, Chem. Sustainable Dev. **10**, 733 (2002).
34) Y. Jiang, M. Liu, Y. Wang, H. Song, J. Gao, and G. Meng, J. Phys. Chem. A **110**, 13479 (2006).
35) J. E. Noakes, A. Arrott, and C. Haakana, Rev. Sci. Instrum. **39**, 1436 (1968).
36) S. Foner, J. Appl. Phys. **79**, 4740 (1996).
37) T. Yoshitake, D. Nakagauchi, and K. Nagayama, Jpn. J. Appl. Phys. **42**, L849 (2003).
38) L. P. Carignan, R. W. Cochrane, and D. Ménard, Rev. Sci. Instrum. **79**, 035107 (2008).
39) H. St. C. O'Neill and W. A. Dollase, Phys. Chem. Miner. **20**, 541 (1994).
40) E. W. McFarland and J. Tang, Nature **421**, 616 (2003).